Cascading Failures as Continuous Phase-Space Transitions

Yang Yang[1] and Adilson E. Motter[1,2,*]
[1]Department of Physics and Astronomy, Northwestern University, Evanston, Illinois 60208, USA
[2]Northwestern Institute on Complex Systems, Northwestern University, Evanston, Illinois 60208, USA
(Received 7 September 2016; revised manuscript received 1 June 2017; published 14 December 2017)

In network systems, a local perturbation can amplify as it propagates, potentially leading to a large-scale cascading failure. Here we derive a continuous model to advance our understanding of cascading failures in power-grid networks. The model accounts for both the failure of transmission lines *and* the desynchronization of power generators and incorporates the transient dynamics between successive steps of the cascade. In this framework, we show that a cascade event is a phase-space transition from an equilibrium state with high energy to an equilibrium state with lower energy, which can be suitably described in a closed form using a global Hamiltonian-like function. From this function, we show that a perturbed system cannot always reach the equilibrium state predicted by quasi-steady-state cascade models, which would correspond to a reduced number of failures, and may instead undergo a larger cascade. We also show that, in the presence of two or more perturbations, the outcome depends strongly on the order and timing of the individual perturbations. These results offer new insights into the current understanding of cascading dynamics, with potential implications for control interventions.

DOI: 10.1103/PhysRevLett.119.248302

Cascading processes underlie a myriad of network phenomena [1], including blackouts in power systems [2,3], secondary extinctions in ecosystems [4,5], and complex contagion in financial networks [6,7]. In all such cases, an otherwise small perturbation may propagate and eventually cause a sizable portion of the system to fail. Various system-independent cascade models have been proposed [8–13] and used to draw general conclusions, such as on the impact of interdependencies [14] and countermeasures [15]. There are outstanding questions, however, for which it is necessary to model the cascade dynamics starting from the actual dynamical state of the system.

In power-grid networks, the state of the system is determined by the power flow over transmission lines and the frequency of the power generators, which must be, respectively, below capacity and synchronized under normal steady-state conditions. Although a local perturbation has limited impact on the connectivity of the network, it may trigger a cascade of failures and protective responses that switch off grid components and may also lead generators to lose synchrony. Much of our current understanding about this process has been derived from quasi-steady-state cascade models [16–21], which use iterative procedures to model the successive inactivation of network components caused by power flow redistributions, while omitting the transient dynamics between steady states as well as the dynamics of the generators. Further understanding has resulted from stability studies focused on the synchronization dynamics of power generators in the absence of flow redistributions [22–26].

Yet, to date no theoretical approach has been developed to incorporate at the same time these two fundamental aspects of power-grid dynamics—frequency change and flow redistribution—in the modeling of cascading failures [27]. The goal of our study is to fill this gap and consider the interaction between these two factors. Our framework is inspired by energy function analysis approaches considered in the study of power system stability [28,29] and of bistability of circuit elements [30].

Specifically, in this Letter, we introduce a time-continuous cascade model that includes the dynamics of the state variables—governed by the swing equations of the generators, frequency dependence of loads, and power flow equations—as well as the dynamics of the status variables describing the on-off (i.e., operational-disabled) condition of the transmission lines. Within this model, the steady operating states of the system correspond to stable equilibria, and a cascade event is a phase-space transition from one stable equilibrium to another. We study these states and show that the stable equilibria are the local minima of an energylike function. This leads to numerous important implications that have not been systematically studied before. In particular, it follows from the properties of this function that a perturbed system cannot always reach the equilibrium state predicted by quasi-steady-state models and may instead approach an equilibrium corresponding to a larger cascade; this highlights the importance of the dynamics between successive steps of a cascade, as considered in our continuous model, which is a factor that has remained unexplored with few exceptions [1,31–33]. It also follows that the equilibrium energy does not depend monotonically on the number of failures and that cascades triggered by multiple perturbations depend strongly on the perturbation order. These results suggest the possibility of cascade mitigation using judiciously designed perturbations to steer the system to a preferred equilibrium that would not be reached spontaneously.

We first consider the protective operation, common to most power networks, that *removes* a transmission line when the flow on it exceeds its capacity. We associate each line ℓ with a continuous variable η_ℓ representing its on-off status (as well as the continuous process of switching between the two conditions) and a parameter λ_ℓ indicating the fraction of the line capacity used by the flow. As shown below, this allows us to incorporate the line status into the dynamical equations by scaling the power flow terms by η_ℓ, with η_ℓ representing the normal status for $\lambda_\ell < 1$ and the failed status for $\lambda_\ell \geq 1$, where η_ℓ is thus constrained to the unit interval. To model the automatic removal of the overloaded lines, we can then define the dynamics of η_ℓ as

$$\dot{\eta}_\ell = f(\eta_\ell) - \lambda_\ell, \tag{1}$$

where the rhs is defined to satisfy three physical conditions: (I) for $\lambda_\ell < 1$, there are three equilibria $\eta_\ell^{(f)} < \eta_\ell^{(c)} < \eta_\ell^{(n)}$, where $\eta_\ell^{(n)} \approx 1$ is a stable equilibrium representing the normal operation status, $\eta_\ell^{(f)} \approx 0$ is a stable equilibrium representing the failed status, and $\eta_\ell^{(c)}$ is an unstable equilibrium marking the critical value below which η_ℓ evolves to the failed status; (II) for $\lambda_\ell \geq 1$, only the equilibrium $\eta_\ell^{(f)}$ remains stable, which is satisfied if the local maximum of f in $(\eta_\ell^{(c)}, \eta_\ell^{(n)})$ is 1; (III) $\eta_\ell^{(c)}$ is always close to 1, since a line should be fully operational under normal conditions. The dynamics does not depend sensitively on the details of function f provided these conditions are satisfied. Throughout, we use overdot to indicate time derivative.

Here we define $f(\eta_\ell) = a^{-1}[{\eta_\ell}^{-1} - (1-\eta_\ell)^{-1}] + a\eta_\ell^4 - b$, where a and b are positive parameters. The terms ${\eta_\ell}^{-1}$ and $-(1-\eta_\ell)^{-1}$ constrain η_ℓ above 0 and below 1, respectively, as they ensure that $f(\eta_\ell) \to \infty$ for $\eta_\ell \to 0^+$ and $f(\eta_\ell) \to -\infty$ for $\eta_\ell \to 1^-$. The term η_ℓ^4 allows f to have three roots—corresponding to $\eta_\ell^{(f)}$, $\eta_\ell^{(c)}$, and $\eta_\ell^{(n)}$ for $\lambda_\ell = 0$, as shown in Fig. 1(a). The parameters a and b are adjustable to set $\eta_\ell^{(f)}$ close to 0, to set $\eta_\ell^{(c)}$ and $\eta_\ell^{(n)}$ sufficiently close to 1, and to set the local maximum of f to 1. For this choice of function f, Eq. (1) satisfies conditions (I)–(III). Moreover, the equation can be rewritten as a gradient system $\dot{\eta}_\ell = -d\phi(\eta_\ell)/d\eta_\ell$, where $\phi(\eta_\ell) = \lambda_\ell \eta_\ell - F(\eta_\ell)$, and $dF(\eta_\ell)/d\eta_\ell = f(\eta_\ell)$. As shown in Fig. 1(b), the stable equilibria of this system correspond to the local minima of $\phi(\eta_\ell)$.

Following a perturbation, the power flowing on transmission lines can change dynamically. When the flow on line ℓ reaches its capacity ($\lambda_\ell \geq 1$), the system will experience a saddle-node bifurcation and the status variable η_ℓ will evolve to the stable equilibrium $\eta_\ell^{(f)}$, representing a line switch-off operation. This is a one-way action, since the equilibrium $\eta_\ell^{(f)}$ is stable for any value of λ_ℓ.

Having defined the dynamics of the status variables, we now incorporate the system's protective response into the dynamical equations governing the state of the network. In a network of n nongenerator nodes, each such node is an electric point where power is extracted by a load, received from generators, and/or redistributed among transmission lines. We denote by n_g the number of generators and by n_l the number of transmission lines. To proceed, we consider the extended representation of the network [37] in which each generator is now an additional node connected to the network through a virtual line (not included in n_l and not subject to failure), leading to a network of $n + n_g$ nodes. For notational convenience, we reindex the generators as the first n_g nodes.

Assuming that the voltage satisfies $|V_i| \approx 1$ (in per unit) for all nodes and that no real power is lost on transmission lines, we can define the state of a power system as $\mathbf{x} = (\boldsymbol{\omega}, \boldsymbol{\delta}, \boldsymbol{\eta})$. Here, $\boldsymbol{\omega} = (\omega_i)$ are the frequencies of the generators relative to the system's nominal frequency, $\boldsymbol{\delta} = (\delta_i)$ are the phase angles of all other nodes relative to a reference node (taken to be $i = 1$, so that $\delta_1 \equiv 0$), and $\boldsymbol{\eta} = (\eta_\ell)$ are the status variables of the (nonvirtual) transmission lines $\mathcal{L}$, where $\ell \in \mathcal{L}$. The state of the system is suitably determined by the following equations:

$$\begin{aligned}
&\dot{\omega}_i = -\frac{D_i}{M_i}\omega_i - \frac{1}{M_i}\left(P_i + \sum_{j=n_g+1}^{n_g+n} \tilde{B}_{ij}\sin\delta_{ij}\right), && i = 1, 2, \ldots, n_g,\\
&\dot{\delta}_i = \omega_i - \omega_1, && i = 2, \ldots, n_g,\\
&\dot{\delta}_i = -\frac{1}{T_i}\left(P_i + \sum_{j=1}^{n_g} \tilde{B}_{ij}\sin\delta_{ij} + \sum_{j=n_g+1}^{n_g+n} \tilde{B}_{ij}\eta_{\ell_{i\text{-}j}}\sin\delta_{ij}\right) - \omega_1, && i = n_g+1, \ldots, n_g+n,\\
&\dot{\eta}_{\ell_{i\text{-}j}} = 10\left(f(\eta_{\ell_{i\text{-}j}}) - \frac{\tilde{B}_{ij}(1-\cos\delta_{ij})}{W_{\ell_{i\text{-}j}}}\right), && \ell_{i\text{-}j} \in \mathcal{L}.
\end{aligned} \tag{2}$$

Here, $\delta_{ij} = \delta_i - \delta_j$ and $\tilde{B}$ is a symmetric matrix with nonzero elements $\tilde{B}_{ij} = -1/x_{\ell_{i\text{-}j}}$, where $x_{\ell_{i\text{-}j}}$ is the transient reactance of a generator or is the reactance of a transmission line, depending on whether the line connecting i and j is virtual or not. The first two equations are the swing equations describing the dynamics of the generators, where M_i is the generator rotor inertia, D_i is the rotor damping ratio, and P_i is the negative of the mechanical power input $P_i^{(m)}$ of the generator [38]. The third equation describes loads (and nongenerator nodes in general, under the assumption

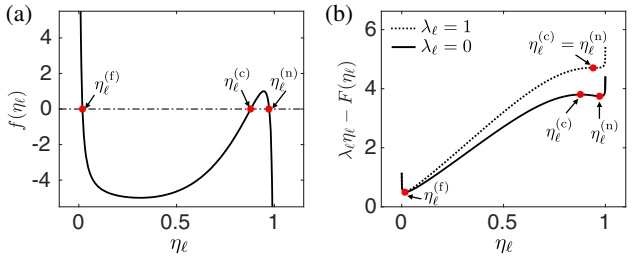

FIG. 1. Line-status switch model. (a) Function $f(\eta_\ell)$ for $a = 10$, whose roots are the equilibrium points of Eq. (1) when $\lambda_\ell = 0$ (for other values of λ_ℓ, see Fig. S1 in Supplemental Material [34]). (b) Potential function $\phi(\eta_\ell) = \lambda_\ell\eta_\ell - F(\eta_\ell)$, where the local minima for $\lambda_\ell = 0$ correspond to the stable equilibria in (a). When λ_ℓ is increased past 1, the local minimum $\eta_\ell^{(n)}$ merges with $\eta_\ell^{(c)}$ and then disappears.

that they include some frequency-dependent power exchange) as first-order rotors, where T_i is the load frequency ratio and P_i is the power $P_i^{(d)}$ demanded at the node. We further assume that $\sum_{i=1}^{n_g+n} P_i = 0$, so that there exists an equilibrium point at $\omega_i = 0$ and $\delta_i = cte$. Note that the term representing the power flow on line $\ell_{i\text{-}j}$ is multiplied by the status variable $\eta_{\ell_{i\text{-}j}}$, which automatically turns off the line in the event of an overload (when $\eta_\ell \to \eta_\ell^{(f)}$). The last equation describes the dynamics of the status variables, where $\lambda_{\ell_{i\text{-}j}}$ in Eq. (1) is replaced by $\tilde{B}_{ij}(1 - \cos\delta_{ij})$, the reactance energy stored in the transmission line $\ell_{i\text{-}j}$, divided by $W_{\ell_{i\text{-}j}}$, the maximum reactance energy that line $\ell_{i\text{-}j}$ can hold. The prefactor 10 in this equation assures that the time scale for line failures is much shorter than that of the other dynamical changes in the network. For more details on the derivation of Eq. (2), see Supplemental Material [34].

Importantly, we can show that Eq. (2) can be derived from a Hamiltonian-like system of the form

$$\dot{\mathbf{x}} = J\nabla\Psi(\mathbf{x}), \tag{3}$$

where $\Psi(\mathbf{x})$ is an energy function defined as

$$\begin{aligned}\Psi(\mathbf{x}) = &\sum_{i=1}^{n_g}\left[\frac{1}{2}M_i\omega_i^2 + \sum_{j=n_g+1}^{n_g+n}\tilde{B}_{ij}(1-\cos\delta_{ij})\right] \\ &+ \sum_{i=n_g+1}^{n_g+n}\sum_{j=i+1}^{n_g+n}\tilde{B}_{ij}(1-\cos\delta_{ij})\eta_{\ell_{i\text{-}j}} \\ &+ \sum_{i=2}^{n_g+n}P_i\delta_i - \sum_{\ell_{i\text{-}j}\in\mathcal{L}}W_{\ell_{i\text{-}j}}F(\eta_{\ell_{i\text{-}j}})\end{aligned} \tag{4}$$

and J is a matrix of the form

$$J = \begin{bmatrix} J_{11} & J_{12} & J_{13} & \mathbf{0} \\ -J_{12}^T & \mathbf{0} & \mathbf{0} & \mathbf{0} \\ -J_{13}^T & \mathbf{0} & J_{33} & \mathbf{0} \\ \mathbf{0} & \mathbf{0} & \mathbf{0} & J_{44} \end{bmatrix}. \tag{5}$$

In this matrix, the off-diagonal blocks are

$$J_{12} = \begin{bmatrix} \frac{1}{M_1} & \frac{1}{M_1} & \cdots & \frac{1}{M_1} \\ \frac{-1}{M_2} & 0 & \cdots & 0 \\ 0 & \frac{-1}{M_3} & \cdots & 0 \\ \vdots & \vdots & \ddots & \vdots \\ 0 & 0 & \cdots & \frac{-1}{M_{n_g}} \end{bmatrix}, \qquad J_{13} = \begin{bmatrix} \frac{1}{M_1} & \cdots & \frac{1}{M_1} \\ 0 & \cdots & 0 \\ \vdots & \vdots & \vdots \\ 0 & \cdots & 0 \end{bmatrix}, \tag{6}$$

and the diagonal blocks are

$$\begin{aligned} J_{11} &= \mathrm{diag}\left(-\frac{M_1}{D_1^2}, -\frac{M_2}{D_2^2}, \ldots, -\frac{M_{n_g}}{D_{n_g}^2}\right), \\ J_{33} &= \mathrm{diag}\left(-\frac{1}{T_{n_g+1}}, -\frac{1}{T_{n_g+2}}, \ldots, -\frac{1}{T_{n_g+n}}\right), \\ J_{44} &= 10\times\mathrm{diag}\left(-\frac{1}{W_1}, -\frac{1}{W_2}, \ldots, -\frac{1}{W_{n_l}}\right). \end{aligned} \tag{7}$$

For details on the derivation of Eq. (3), see Supplemental Material [34].

Crucially, the matrix J is the sum of a skew-symmetric matrix and a diagonal matrix with nonpositive elements, from which we can show that $d\Psi(\mathbf{x}(t))/dt = \nabla\Psi(\mathbf{x})^T\dot{\mathbf{x}} = \nabla\Psi(\mathbf{x})^T J\nabla\Psi(\mathbf{x}) \le 0$. Moreover, because J is also full rank (which follows from its reduced row echelon form), we have that $d\Psi(\mathbf{x}(t))/dt = \mathbf{0}$ if and only if $\nabla\Psi(\mathbf{x}) = \mathbf{0}$, and hence if and only if $\dot{\mathbf{x}} = J\nabla\Psi(\mathbf{x}) = \mathbf{0}$. Thus, when the network is perturbed, the energy function $\Psi(\mathbf{x})$ monotonically decreases as the system evolves and becomes constant again only when the system reaches an equilibrium point of Eq. (3) [and hence of Eq. (2)]. Such equilibria represent stable steady states, where the generators are synchronized $[\omega_1(t) = \omega_2(t) = \cdots = \omega_{n_g}(t)]$, the angle differences are fixed for all pairs of nodes, and the flow is below capacity for all operating transmission lines.

We first illustrate our formalism on Iceland's power-grid network, shown in Fig. 2(a) (for parameter setting, see Supplemental Material [34]). The system is designed to have a stable steady state with no additional failures when any single transmission line is missing (provided the network remains connected), which is verified in our simulations. We test whether such a cascade-free steady state is actually reached following the removal of a line when the *transient dynamics* between steady states represented in our model is taken into consideration. Starting from the stable steady state determined by Eq. (2), we simulate all 68 single-line removal perturbations that keep the network topologically connected (performed by changing η_ℓ to $\eta_\ell^{(f)}$). Of these, ten do not converge to the best available stable steady state and instead undergo subsequent failures (Fig. S3 in Supplemental Material [34]). Insights into the underlying mechanism are provided by the

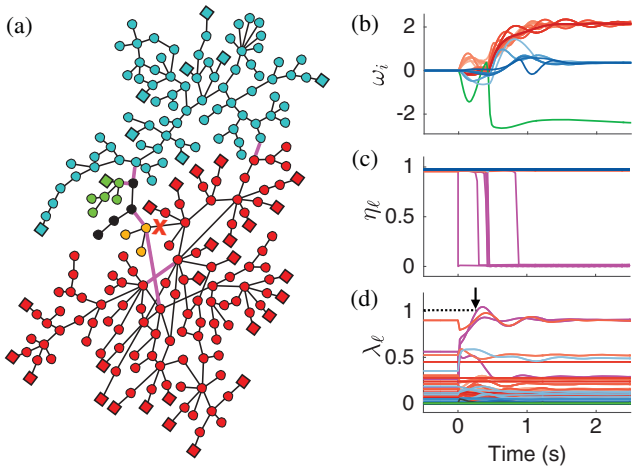

FIG. 2. Simulated cascade event in Iceland's power grid. (a) Diagram of the network, which consists of 35 generators (squares), 189 nongenerator nodes (circles), and 203 transmission lines (line segments) [40]. The removal of the marked line (cross symbol) triggers a sequence of six subsequent line failures (magenta) that separate the network into five clusters (color coded). (b),(c) Corresponding generator frequencies ω_i (b) and line-status variables η_ℓ (c) as functions of time [color coded as in (a)]. (d) Corresponding fraction λ_ℓ of the line capacity used, should the line overloaded at 0.2 s (arrow) not be disabled.

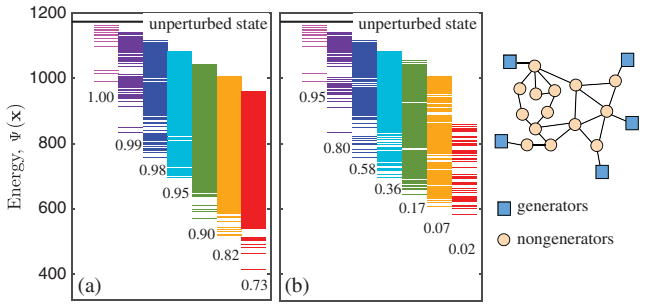

FIG. 3. Energy levels $\Psi(\mathbf{x})$ of the stable states in the 14-bus test system. Each panel shows all combinations of 1 (left column) to 7 (right) successive line removals that leave the network connected. (a) All stable states without additional failures determined using the MATLAB function *fsolve*. (b) Subset of stable states in (a) that the system actually evolves to for the same line removals as in (a). Also marked are the fractions of perturbations for which a stable state is identified (a) and the fractions of those stable states actually reached (b). The diagram on the rhs shows the topology of the network.

example shown in Figs. 2(a)–2(c), where a sequence of line overloads separates the network into five clusters. As shown in Fig. 2(d), the system would eventually have approached the designed steady state with no additional failures, but a line overload—whose automatic switch-off triggers subsequent overloads—occurs before the system can reach that state. In this case, no feasible trajectory exists in the phase space connecting the initial state to the steady state predicted by quasi-steady-state models. This scenario is common in general, as shown for five other systems in the 3rd column of Table S2 (Supplemental Material [34]).

When the network is subject to multiple perturbations, our framework shows that the cascade outcome will generally depend on the order and timing of the perturbations. A natural measure to quantify this difference is the size C' (i.e., number of nodes) of the largest connected cluster in the postcascade stable state. As an illustration, we consider the following three scenarios for two-line removal perturbations: (i) remove line $\ell_{i_1\text{-}j_1}$ and then, after the stable state is reached, remove line $\ell_{i_2\text{-}j_2}$; (ii) the same as in (i) but for $\ell_{i_1\text{-}j_1}$ swapped with $\ell_{i_2\text{-}j_2}$; (iii) remove $\ell_{i_1\text{-}j_1}$ and $\ell_{i_2\text{-}j_2}$ concurrently. Considering all 2117 pairs of lines $(\ell_{i_1\text{-}j_1}, \ell_{i_2\text{-}j_2})$ that keep Iceland's network connected after their removal (but not necessarily after the resulting cascading failures), our simulations indicate that 30.0% of these perturbations lead to cascades in at least one of the scenarios above. For this subset of line pairs, we obtain that: (a) "order matters" in 27.9% of the cases, in that C' differs for at least one of the scenarios; (b) choosing between the orders in (i) and (ii) leads to the largest C' in 20.8% of the cases; (c) (i) and (ii) lead to equally best C' in 4.3% of the cases; (d) the concurrent removal scenario (iii) trumps (i) and (ii) in the remaining 2.8% of the cases (for specific examples, see Figs. S4 and S5 in Supplemental Material [34]). Similar trends are observed for all five other systems considered, as shown in Table S2 (Supplemental Material [34]). This order dependence has potential implications for control, as it can be exploited in proactive line removals to prevent subsequent failures (Fig. S6 in Supplemental Material [34]). This reveals a sharp contrast between processes for which order is immaterial, such as percolation, and the cascades considered here.

Taking the analysis one step further, our formalism offers unique insight into the relation between line removal perturbations and energy levels. Figure 3(a) shows all energy levels for stable steady states of the IEEE 14-bus test system (chosen in place of Iceland's network to avoid a cluttered picture) for all combinations of one to seven line removals that keep the network connected. Figure 3(b) shows the states that the system actually approaches following these successive line removals—the missing states [compared to Fig. 3(a)] are the ones not reached because the system undergoes a cascade.

Two major results follow from this. First, it confirms that upon perturbation the system often does not reach the available stable steady state with smallest number of failures (e.g., for seven line removals, this is so for 98% of all cases). Second, the range of energy levels with $k+1$ line removals overlaps with the range for k line removals. There are, for example, stable steady states with only one line failure at a lower energy than many stable states with 2, 3, …, 6 line failures. This shows that, following a perturbation that could eventually lead to a stable state with multiple failures, the system can in principle be steered to a lower-energy state which has, nevertheless, a reduced number of failures. Crucially, this is possible without

external input of energy, as the system tends to go spontaneously to lower-energy states following a perturbation.

In summary, the model presented here accounts—in a single phase space—for the interaction between the full dynamics of a cascade (including transients) and the changes to the underlying network structure imposed by the resulting failures. The results explain the combinatorial impact of perturbations, identify conditions under which a cascade may develop despite the presence of a stable state that would withstand the perturbation, and suggest new opportunities for cascade control.

The authors thank Takashi Nishikawa for feedback on the manuscript. This work was supported by an Institute for Sustainability and Energy at Northwestern (ISEN) Booster Award, National Science Foundation (NSF) Grant No. DMS-1057128, Simons Foundation Award No. 342906, and Advanced Research Projects Agency-Energy (ARPA-E) Award No. DE-AR0000702. The views and opinions of authors expressed herein do not necessarily state or reflect those of the United States Government or any agency thereof.

*motter@northwestern.edu

[1] A. E. Motter and Y. Yang, Phys. Today **70**, No. 1, 32 (2017).
[2] R. Liscouski *et al.*, Final Report on the August 14, 2003 Blackout in the United States and Canada: Causes and Recommendations, 2004.
[3] F. Vandenberghe *et al.*, Final Report of the Investigation Committee on the 28 September 2003 Blackout in Italy, 2004.
[4] J. A. Dunne and R. J. Williams, Phil. Trans. R. Soc. B **364**, 1711 (2009).
[5] S. Sahasrabudhe and A. E. Motter, Nat. Commun. **2**, 170 (2011).
[6] P. Gai and S. Kapadia, Proc. R. Soc. A **466**, 2401 (2010).
[7] M. Elliott, B. Golub, and M. O. Jackson, Am. Econ. Rev. **104**, 3115 (2014).
[8] D. J. Watts, Proc. Natl. Acad. Sci. U.S.A. **99**, 5766 (2002).
[9] A. E. Motter and Y.-C. Lai, Phys. Rev. E **66**, 065102(R) (2002).
[10] K.-I. Goh, D.-S. Lee, B. Kahng, and D. Kim, Phys. Rev. Lett. **91**, 148701 (2003).
[11] P. Crucitti, V. Latora, and M. Marchiori, Phys. Rev. E **69**, 045104 (2004).
[12] S. V. Buldyrev, R. Parshani, G. Paul, H. E. Stanley, and S. Havlin, Nature (London) **464**, 1025 (2010).
[13] C. D. Brummitt, G. Barnett, and R. M. D'Souza, J. R. Soc. Interface **12**, 20150712 (2015).
[14] C. D. Brummitt, R. M. D'Souza, and E. A. Leicht, Proc. Natl. Acad. Sci. U.S.A. **109**, E680 (2012).
[15] A. E. Motter, Phys. Rev. Lett. **93**, 098701 (2004).
[16] I. Dobson, B. A. Carreras, V. E. Lynch, and D. E. Newman, Chaos **17**, 026103 (2007).
[17] M. Anghel, K. A. Werley, and A. E. Motter, in *Proceedings of the 40th Annual HICSS* (IEEE, New York, 2007), Vol. 1, p. 113.
[18] D. Watts and H. Ren, in *Proceedings of the 2008 IEEE International Conference on Sustainable Energy Technology* (IEEE, New York, 2008), p. 1200.
[19] R. D. Zimmerman, C. E. Murillo-Snchez, and R. J. Thomas, IEEE Trans. Power Syst. **26**, 12 (2011).
[20] D. Witthaut, M. Rohden, X. Zhang, S. Hallerberg, and M. Timme, Phys. Rev. Lett. **116**, 138701 (2016).
[21] A. Moussawi, N. Derzsy, X. Lin, B. K. Szymanski, and G. Korniss, Sci. Rep. **7**, 11729 (2017).
[22] Y. Susuki, I. Mezić, and T. Hikihara, J. Nonlinear Sci. **21**, 403 (2011).
[23] M. Rohden, A. Sorge, M. Timme, and D. Witthaut, Phys. Rev. Lett. **109**, 064101 (2012).
[24] A. E. Motter, S. A. Myers, M. Anghel, and T. Nishikawa, Nat. Phys. **9**, 191 (2013).
[25] F. Dörfler, M. Chertkov, and F. Bullo, Proc. Natl. Acad. Sci. U.S.A. **110**, 2005 (2013).
[26] P. J. Menck, J. Heitzig, J. Kurths, and H. J. Schellnhuber, Nat. Commun. **5**, 3969 (2014).
[27] Theoretical understanding is especially needed given that available reports of empirical data on cascade blackouts generally do not include detailed information about generator behavior along with power flow information.
[28] A. R. Bergen and D. J. Hill, IEEE Trans. Power Appar. Syst. **PAS-100**, 25 (1981).
[29] A. Pai, *Energy Function Analysis for Power System Stability* (Springer, New York, 2012).
[30] C. L. DeMarco, IEEE Control Syst. Mag. **21**, 40 (2001).
[31] I. Simonsen, L. Buzna, K. Peters, S. Bornholdt, and D. Helbing, Phys. Rev. Lett. **100**, 218701 (2008).
[32] S. P. Cornelius, W. L. Kath, and A. E. Motter, Nat. Commun. **4**, 1942 (2013).
[33] B. Schäfer, D. Witthaut, M. Timme, and V. Latora, arXiv:1707.08018.
[34] See Supplemental Material at http://link.aps.org/supplemental/10.1103/PhysRevLett.119.248302, which includes Refs. [35,36], for details of the analysis and additional examples.
[35] H. Zheng and C. L. DeMarco, in *Proceedings of the North American Power Symposium, 2010* (IEEE, New York, 2010), p. 1.
[36] F. Milano, IEEE Trans. Power Syst. **20**, 1199 (2005).
[37] T. Nishikawa and A. E. Motter, New J. Phys. **17**, 015012 (2015).
[38] These equations follow from Newton's second law applied to the generator rotor [39]: $I_i\dot{\omega}_i = -\tilde{D}_i\omega_i + (\mathcal{T}_i^{(m)} - \mathcal{T}_i^{(e)})$, where I_i is the moment of inertia, $\tilde{D}_i$ is the damping coefficient, $\mathcal{T}_i^{(m)}$ is the mechanical torque, and $\mathcal{T}_i^{(e)}$ is the torque due to electrical load in the network. Thus, $M_i = (\omega_o/P_o)I_i$, $D_i = (\omega_o/P_o)\tilde{D}_i$, $P_i^{(m)} = [(\omega_i + \omega_o)/P_o]\mathcal{T}_i^{(m)}$, and $\sum_{j=n_g+1}^{n_g+n} \tilde{B}_{ij}\sin\delta_{ij} = [(\omega_i + \omega_o)/P_o]\mathcal{T}_i^{(e)}$, where the relative frequency ω_i is assumed to be small compared to the nominal frequency ω_o, and the base power P_o is used to transform the power terms into per unit quantities.
[39] J. J. Grainger and W. D. Stevenson, *Power System Analysis* (McGraw-Hill, New York, 1994).
[40] Iceland's transmission network, http://www.maths.ed.ac.uk/optenergy/NetworkData/howtouse.html (accessed: 2016-05-18).